ASME Journal of Autonomous Vehicles and Systems
Online journal at:
https://asmedigitalcollection.asme.org/autonomousvehicles

Christopher Goodin[1]
Associate Research Professor
Center for Advanced Vehicular Systems,
Mississippi State University,
Starkville, MS 39759
e-mail: cgoodin@cavs.msstate.edu

Greg Henley
Center for Advanced Vehicular Systems,
Mississippi State University,
Starkville, MS 39759

Lucas Cagle
Center for Advanced Vehicular Systems,
Mississippi State University,
Starkville, MS 39759

Brandon Black
Center for Advanced Vehicular Systems,
Mississippi State University,
Starkville, MS 39759

Justin Carrillo
Mobility Systems Branch,
U.S. Army Engineer Research and Development Center,
Vicksburg, MS 39180

David McInnis
Mobility Systems Branch,
U.S. Army Engineer Research and Development Center,
Vicksburg, MS 39180

Decentralized Swarm Control in Communication-Constrained Environments Using a Blended Leader Follower-Artificial Potential Field With Biologically Inspired Interactions

This paper presents a study of how communication ranges influence the performance of a new decentralized control method for swarms of autonomously navigating ground vehicles that uses a blended leader–follower/artificial potential field approach. While teams of autonomous ground vehicles (AGVs) that can navigate autonomously through off-road terrain have a variety of potential uses, it may be difficult to control the team in low-infrastructure environments that lack long-range radio communications capabilities. In this work, we propose a novel decentralized swarm control algorithm that combines the potential field planning method with the leader–follower (LF) control algorithm and biologically inspired inter-robot interactions to effectively control the navigation of a team of AGV (swarm) through rough terrain using only a single lead vehicle. We use simulated experimentation to demonstrate the robustness of this approach using only point-to-point wireless communication with realistic communication ranges. Furthermore, we analyze the range requirements of the communication network as the number in the swarm increases. We find that wireless communication range must increase as the number of agents in the swarm increases in order to effectively control the swarm. Our analysis showed that mission success decreased by 40% when the communication range was reduced from 100 m to 200 m, with the exact reduction also depending on the number of vehicles.
[DOI: 10.1115/1.4065533]

Keywords: communication, teaming behaviors, vehicle autonomy

1 Introduction

Self-driving vehicles, also known as autonomous ground vehicles (AGVs), are becoming more and more common. The capabilities of these vehicles are improving over time [1,2]. However, this progress has mostly been limited to highway driving; off-road operation by AGV has been an enduring challenge in the field of autonomy [3]. AGV operating in off-road environments are hampered by the lack of infrastructure. In the case of teams of AGV operating in collaboration (swarms), this includes the lack of infrastructure to support inter-vehicle communication.

Swarms of robots operating collaboratively have been studied extensively in recent years [4]. Past work on biologically inspired algorithms has shown promise for controlling teams of AGV because they use simple interaction rules to create complex emergent behavior [5,6]. However, as robot swarms become more prevalent and grow in size, practical concerns may become a limiting factor in the effectiveness of actually implementing AGV swarms. Specifically, the human–swarm interaction becomes more challenging [7] and inter-robot communication is more demanding [8].

In this work, we propose a solution for control of a multi-AGV swarm navigating through off-road terrain by implementing a blended LF and artificial potential field (APF) control algorithms that use biologically inspired swarm interaction algorithms to maintain formation spacing. The biological term in our algorithm uses the "attention-based" interaction term from Ref. [9], an approach which has not been taken in any previous implementations of the APF. In our approach, the lead vehicle is controlled by a human driver while the remaining vehicles move in an APF that is modified not only by the terrain but also by the lead vehicle and other vehicles in the swarm. The vehicles are only required to communicate their position to the other vehicles via point-to-point radio communication. We demonstrate the viability of this solution using a

[1]Corresponding author.

Manuscript received August 3, 2023; final manuscript received April 18, 2024; published online June 13, 2024. Assoc. Editor: David Gorsich.

physics-based simulator, the Mississippi State University (MSU) autonomous vehicle simulator (MAVS) [10], and analyze the influence of communication range on performance of the swarm. The primary contribution of this work is to study how varying communication range affects the performance of the algorithm as the size of the swarm changes.

In the following sections, we give some background on related research (Sec. 2) and introduce our blended swarm control method (Sec. 3). We use a set of simulated experiments (Sec. 4) to demonstrate the effectiveness of the swarm in performing navigation and maintaining communication and show the dependence of the swarm control on communication range (Sec. 5). Section 6 gives the summary and conclusion.

2 Background and Related Work

This section gives a brief overview of work related to our development of a blended LF-APF control model for swarms of autonomous ground vehicles. The following subsections break down related work in the areas of swarming (Sec. 2.1), leader–follower control (Sec. 2.2), and finally a problem statement for this work (Sec. 2.3).

2.1 Autonomous Swarms. Studies in cooperative robotics have mainly depended on behavior-based control for robots. This behavior-based paradigm has been influential due to it being biologically inspired [11]. A common application for biologically inspired control is in cooperative multi-robot systems, where rules from biological systems are applied to artificial systems to produce organized interactions with intelligent behavior [12]. Robotics researchers examine the social characteristics of insects and animals and apply their discoveries to the design of multi-robot systems [13]. Barnes et al. [14] used potential fields for group control of AGV. They demonstrated their method with field experiments.

Burgard et al. studied multi-robot exploration of an indoor space using a team of two robots [15,16]. Later work in a similar vein came from several sources such as Refs. [17–20].

Eberhart and Kennedy discovered an optimization method based on the swarming theory in simulations [21]. They showed the effectiveness of a method known as the particle swarm optimization (PSO) method. This method was widely adopted and adapted to a variety of scenarios and tests. For example, Hereford and Siebold developed a version of the PSO method known as physically embedded PSO [22]. It was designed to control a swarm as it searched for a target in an environment. There were also modifications made for space exploration [23]. Similarly, Mabrouk and McInnes [24] developed a method for negotiating complex obstacles with a swarm in which the individual agents were able to modify the local potential based on their perceived progress toward a goal point. Additionally, Dunbar and Esposito [25] developed a swarm control method which optimized the connectivity of the swarm in addition to making progress toward a goal point. More recently, Elkilany et al. [26] performed multi-objective optimization with a swarm that could avoid obstacles, maintain formation, and track a desired trajectory.

Other researchers have designed algorithms to resemble different insects and animals. Reynolds created a computer simulation of artificial birds that could represent the motion of birds flocking using simple rules [27]. Dorigo et al. proposed an optimization method that resembled an ant colony [28]. Ward et al. created artificial fish that resembled a schooling behavior that fish use [29].

Advances and adoption in high-performance computing (HPC) have also permitted more expansive simulations of biologically based control algorithms [30]. This includes recent work on negative obstacle detection by AGV swarms [31]. While these past works advanced the state of knowledge on multi-robot control, in this work multi-robot control is integrated with a leader–follower algorithm to mitigate potential limitations related to global planning for swarms by allowing a human-driven leader to determine the global path.

Table 1 Summary of the literature review

Reference	Description
Swarms	
[11–14]	Behavior-based
[15–20]	Indoor exploration
[21–26]	Swarm optimization
[27–29,31]	Biological control
Leader–follower	
[32,33]	Direct connection
[34–37]	With swarms/fuzzy
[39,40]	Decentralized
Potential field	
[41–46]	Global
[47–49]	Local
[50,51]	With kinematics

2.2 Leader–Follower Control. The leader–follower approach is a commonly used method for controlling a group of robots. In this approach, the vehicle is designated as the leader is manually controlled or follows a predefined trajectory while the other vehicles (followers) maintain a desired distance and orientation to the leader [32]. The advantage of using this approach is its simplicity. The leader is the only vehicle which requires sophisticated control, from a human operator or otherwise; the other vehicles simply communicate with and follow the leader [33].

Dehghani et al. measured kinematic parameters on a swarm of vehicles to enhance the leader–follower approach by helping these swarms maintain formation during specific tasks [34]. Miah implemented the leader follower approach for area surveillance using a swarm of vehicles [35]. Miah used radio sensors for the vehicles to communicate their orientation and positioning to map out the given area. Tutuko et al. created a non-holonomic leader–follower model that emphasizes fuzzy logic [36]. Fuzzy logic is used to handle any uncertainty that could happen during operation [37]. It is used during cases like unexpected vehicle collisions or a follower losing connection with the leader. Many of these experiments are conducted using the robot operating system (ROS) to allow the followers and the leaders to easily communicate [38].

Leader–follower algorithms can be divided into two categories: centralized and decentralized. While centralized approaches emphasize a single leader, decentralized communication utilizes each robot equally. de Souza Neto and Romero implemented the leader–follower approach with drones using a decentralized version of the leader–follower approach [39]. Zhang et al. used a decentralized adaptive control scheme that differs from the common leader–follower approach by implementing a hidden leader [40]. The followers are unaware as to which robot is the leader. This contrasts with typical centralized cases, in which the leader of the fleet of vehicles is given a path planning algorithm that determines the best path for the leader.

Artificial potential field path planning algorithm pairs well with the leader–follower approach for calculating leader trajectories [41]. The goal of a path planning algorithm is to discover a safe and collision-free path accomplishing a given task in a complex environment [42]. Autonomous robot path planning is crucial to robot control systems and has been extensively researched [43,44]. Like the leader follower approach, potential field path planning can be broken up into two main categories: global path planning and local path planning [45]. Global path planning is based on a known environment while local path planning relies solely on sensor data. There are limits to local and global path planners. Potential fields have been used for robot path planning in both the global and local domains [46].

Khatib proposed an APF, which is a local path planning developed for robotic arms to discover a collision-free path [47]. This method performed so well that researchers began using it for vehicles as well. Zhang et al. created a local path planning fusion algorithm by combining the APF and a rolling window method [48]. They used this fusion algorithm to design a path planning for unmanned underwater vehicles. Imran and Kunwar developed a path planner that uses characteristics from local path planning and global path planning to create a near optimal path [49].

There are drawbacks to these potential fields because there are factors that cannot be taken into consideration. Ji et al. proposed a three-dimensional potential field that can overcome these drawbacks and take in constraints such as vehicle kinematics [50]. In comparison, Ragavan et al. used a waypoint navigation system that created points for a vehicle to travel to [51].

Table 1 gives a summary of the references discussed in this section for convenience to the reader.

2.3 Problem Formulation. In light of the prior research presented above, in the following section a control method for a swarm of self-driving unmanned ground vehicle (UGV) is presented. In this scenario, the lead vehicle is driven by a human (not autonomous) and a varying number of following vehicles are tasked to follow the lead vehicle while moving through uneven terrain. Communication with a centralized control system (the lead vehicle) is not guaranteed in this scenario, so control must be decentralized. Only point-to-point communication between the vehicles is available, provided they are within communication range. Therefore, the communication range may greatly influence the overall behavior of the multi-vehicle system. The follower vehicles move in a potential field that is based on a priori map information, the movement of other vehicles in their communication radius (this is the biologically inspired interaction), and the location and speed of the lead vehicle. The metric for success is reaching the goal area with the lead vehicle.

3 Blended Swarm Control Method

Mobile robot path planning using potential fields has been an active field for several decades now [52–54]. The basic premise of all APF planners is similar; obstacles create a repulsive potential on the robot, and the strength of the field is inversely related to the distance. Many publications with different variations on how the obstacles are represented and the exact functional dependence on the obstacle distance have been proposed [55]. In this work, we use a grid-based approach for obstacle representation. Our approach is similar to using an occupancy grid [56,57], except the scalar value associated with each grid cell represents the estimated severity of the obstacle (i.e., a cost map) rather than the probability of the cell being occupied.

While on-road or laboratory AGV often deal with discrete obstacles, in off-road driving there may be a continuum of cost associated with navigating certain areas. In this case, the occupancy grid—where each cell is either occupied or unoccupied by an obstacle—becomes a cost map [58] where each map cell has a certain navigation "cost" associated with traversing that cell. In this work, we use the cost map approach to represent the terrain, and the repulsive potential of each cell is proportional to the cost associated with that cell. We take the terrain cost to be a priori map information in these experiments, although it is possible to buildup a cost map in real-time in off-road AGV navigation [59].

3.1 LF-APF Model. In this work, we modify the traditional APF described above by adding three new terms to the field—a term that represents the attractive potential of the leader, a term representing the repulsive potential of the other AGV in the swarm (to avoid collisions) and a biologically inspired term that represents the attractive potential caused by the motion of the other AGV in the swarm. The resulting potential on vehicle i, $\vec{\phi}_i$ is the sum of the temporally static potential field induced by the terrain ($\vec{\phi}_{i,\mathrm{t}}$), the repulsive field created from the location of the other vehicles in the swarm ($\vec{\phi}_{i,\mathrm{s}}$), the attractive field created by the movement of the other vehicles ($\vec{\phi}_{i,\mathrm{v}}$), and the attractive potential field caused by the leader ($\vec{\phi}_{i,\mathrm{l}}$).

$$\vec{\phi}_i = \vec{\phi}_{i,\mathrm{t}} + \vec{\phi}_{i,\mathrm{s}} + \vec{\phi}_{i,\mathrm{v}} + \vec{\phi}_{i,\mathrm{l}} \tag{1}$$

The terrain induced potential, $\vec{\phi}_{i,\mathrm{t}}$ is found by summing the potential created by all the resistances in the terrain. There are many ways to calculate the terrain resistance that may take into account factors such as the presence of vegetation, terrain roughness, or soil strength [59]. In our previous work, we showed that mapping and perception could be accomplished jointly by the swarm [31]. However, in this work the terrain resistance was simply taken to be proportional to terrain slope, μ. The terrain was gridded in a 2D cost map, such that each grid location on the cost map with index (p, q) and location $\vec{r}_{pq}$ had an associated slope μ_{pq}. The spatially varying terrain potential is then given by

$$\phi_{i,\mathrm{t}} = \sum_{p=0}^{n_p} \sum_{q=0}^{n_q} \frac{\kappa_t \mu_{pq}}{r_{i,pq}^2} \tag{2}$$

where n_p, n_q are the number of cells in the horizontal and vertical directions, respectively, κ_t is the scale of the terrain potential, and $r_{i,pq}$ is the distance from the position of vehicle i to the location of cell (p, q). The dependence on the inverse square of the distance means that only nearby cells have a strong impact on the potential force on the vehicle. Therefore, for computational efficiency we restrict the sums in Eq. (2) to only include cells within a range, $r_{\max}$ of the vehicle. We found $r_{\max} = 25$ m to be a suitable value for this work.

Similarly, the inter-vehicle potential field is created by mapping the potential created by the vehicles onto a 2D grid. The scalar inter-vehicle potential (ϕ_p) at cell location $\vec{r}_{pq}$ is given by

$$\phi_p(\vec{r}_{pq}) = \sum_{j=0}^{n_v} \frac{1}{\vec{r}_{j,pq} - \vec{r}_{\min}} \tag{3}$$

where n_v is the number of vehicles, $r_{j,pq}$ is the distance between vehicle j and cell (p, q), and $r_{\min}$ is the minimum safe vehicle distance. The repulsive vehicle potential is then given by summing over all the cells.

$$\phi_{i,\mathrm{s}} = \kappa_s \sum_{p=0}^{n_p} \sum_{q=0}^{n_q} \frac{\phi_p(\vec{r}_i)}{r_{i,pq}^2} \tag{4}$$

where $r_{i,pq}$ is the distance between vehicle i and cell (p, q) and κ_v is the vehicle potential scale factor. We again restrict the search over cells that are within a range of $r_{\max} = 25$ m for computational efficiency purposes.

The attractive potential exerted on vehicle i by the motion of the other vehicles is given by

$$\vec{\phi}_{i,\mathrm{v}} = \kappa_v \sum_{j=0}^{n_v} w_{ij} \vec{v}_j \tag{5}$$

where $r_{ij} = \|\vec{r}_i - \vec{r}_j\|$, $\vec{v}_j$ is the velocity of vehicle j in m/s, and κ_v is the swarm velocity field scale factor. The biologically inspired attention factor, w_{ij}, is given by

$$w_{ij} = \frac{v_{ij}}{r_{ij}} \tag{6}$$

where $v_{ij} = \|\vec{v}_i - \vec{v}_j\|$. We note that this attention factor means that AGV agents will give more weight (attention) to swarm members whose velocity deviates from their own, and to those

AGV who are closest. This type of biologically inspired swarm interaction is known as attention-based interaction [9]. This biologically based interaction term has not been incorporated into any previous implementations of the APF and is a novel contribution of this work. This approach has the advantage of being totally decentralized—the motion of each autonomous agent is governed only by the motion of the nearby vehicles and works whether a follower has direct communications link with the leader or not.

Finally, the attractive potential on vehicle i induced by the leader vehicle at position r_l is given by

$$\vec{\phi}_{i,l} = -\kappa_l(\vec{r}_i - \vec{r}_l) \tag{7}$$

where κ_l is the leader potential scale factor and $\vec{r}_l$ is the leader position. We note that in contrast to the obstacle potential field which decreases as the inverse distance squared, our proposed leader potential *increases* as the distance increases. This particular form was chosen to encourage agents to minimize the distance between themselves and the leader, i.e., to encourage the followers to "catch up" if they fell behind the leader.

For each vehicle, the desired path for the vehicle was calculated using the total field (Eq. (1)) to iteratively generate a set of waypoints. The distance between waypoints was taken to be one-third of the minimum desired distance between vehicles ($w_d = r_{\min}/3$). Starting from the position of the vehicle, for each point along the desired path $\vec{p}_w$, the next waypoint along the desired path was found from the local direction of the total field.

$$p_{w+1} = p_w + w_d \frac{\vec{\phi}(p_w)}{\|\phi(p_w)\|} \tag{8}$$

A path was generated for each vehicle and used as input into the pure-pursuit control algorithm. The path was updated at each time-step for each vehicle.

The parameters and symbols used in the blended LF-APF control algorithm presented above are summarized in Table 2, along with the values for each parameter used in this work. The values of the potential scalars in Table 2 were determined from trial and error in repeated experimentation and were tuned to give the desired behavior of the follower system. The values for $r_{\min}$ and $r_{\max}$ were chosen based on geometrical considerations of the size and speed of the vehicle. Since the vehicles were traveling at low speeds (5 m/s), obstacles beyond 25 m had little impact on local path planning.

A summary of the LF-APF model is shown in Fig. 1. The LF-APF controller was used for path planning by each vehicle by calculating the total field (Eq. (1)) on the vehicle at a rate of 40 Hz. Each vehicle would receive state updates from all the other vehicles within the communication range. The state updates consisted only of position—the change in position since the last state update would be used to estimate the velocity of the other vehicles in the swarm. Vehicles were identified with an integer ID number, with the lead vehicle having an ID = 0. The updated vehicle positions would be used to update the potential field using the equations described above. With each new field update, the desired global path of the vehicle would be updated to align with the potential field. The remainder of the autonomy stack consisted of a pure-pursuit steering controller and a proportional-integral-derivatve

Table 2 Adjustable model parameters outlined in Sec. 3

Symbol	Description	Value
κ_t	Terrain potential scalar	32.0
κ_s	Repulsive vehicle potential scalar	0.64
κ_v	Vehicle motion potential scalar	16.0
κ_l	Leader potential scalar	16.0
$r_{\min}$	Minimum desired distance between vehicles (m)	16.0
$r_{\max}$	Maximum obstacle search distance around vehicles (m)	25.0

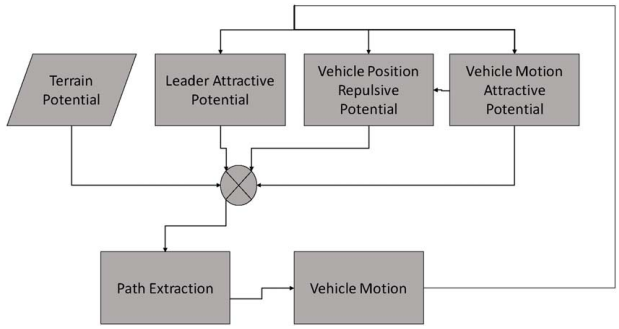

Fig. 1 Flowchart depicting the LF-APF process

(PID) controller for maintaining speed, both of which are described in more detail in Ref. [60]. The terrain map potential field was considered to be known a priori, so no perception module was used in the autonomy stack.

3.2 Radio Communication Model. Communication between the vehicles is simulated as a point-to-point radio network. The simulated radios were 802.11 wireless connections, which may have a range of between 20 and 200 m, depending on the specific wireless local area network (WLAN) protocol [61]. The primary failure mode of these radios which would cause them to lose connection is when the receiver is outside the normal operating range for the WLAN protocol. While the following vehicles in the scenario attempted to maintain a separation distance of less than $r_{\min}$, as the number of vehicles increased, the ranges between any two agents necessarily also increased, leading to connection failures. The radio connections were simulated using a range-based radio model. The probability of connection was modeled using an empirical, range-based approach. In this approach, the inputs to the model are the nominal maximum range of the radio (r_n), the failure rate at that range (f_r), and two times that distance (f_{r2}). For two radios separated by a distance r meters, the connection probability is then given by

$$\sigma(r) = 1 - \frac{1}{1 + e^{-\sigma_g r - \sigma_b}} \tag{9}$$

Equation (9) depends on the gain and bias of the signal. The gain and bias are calculated empirically based on the input ranges and failure rates. The signal gain is

$$\sigma_g = \frac{1}{r_{\max}}\left[\ln\left(\frac{1}{f_r} - 1\right) - \ln\left(\frac{1}{f_{r2}} - 1\right)\right] \tag{10}$$

and the signal bias (σ_b) is

$$\sigma_b = -2\ln\left(\frac{1}{f_r} - 1\right) + \ln\left(\frac{1}{f_{r2}} - 1\right) \tag{11}$$

In this work, we took $f_r = 0.01$ and $f_{r2} = 0.075$. Five different nominal maximum ranges were used in the experiments —$r = 25$, 50, 100, 200, and 500 m. The results of the radio probability of connection for these different maximum ranges are shown in Fig. 2. In the simulations, for two robots separated by a distance r, Eq. (9) was evaluated at every time-step and compared to a random-test variable ranging from zero to one. If the value of Eq. (9) was less than the test variable, the connection was interrupted. This means that for a radio operating at 40 Hz, a failure rate of 97.5% would still yield a successful connection at approximately 1 Hz.

3.3 Advantages and Limitations of LF-APF. There are several limitations of the LF-APF approach outlined above. APF planners are known to struggle with local minima in the potential

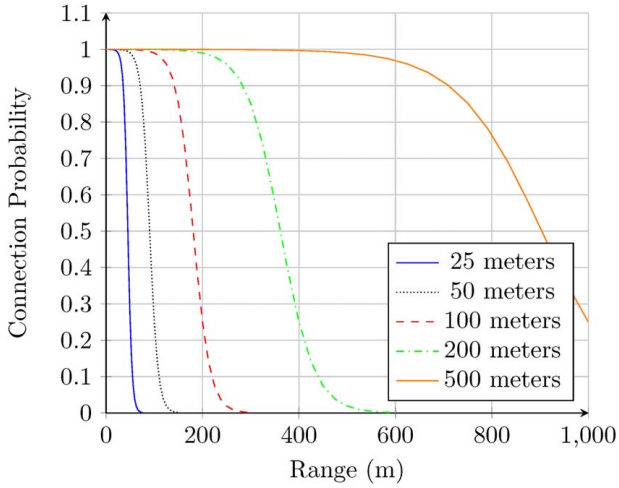

Fig. 2 Radio model relative connection probability versus range for the different nominal max ranges tested in these experiments

field or with horseshoe-shaped obstacles in the terrain. This weakness is mitigated in this work by the incorporation of the "leader–follower" portion of the algorithm. Because the following vehicles are pursuing a human-driven lead vehicle, it can be assumed that the desired path in pursuit of the lead vehicle will avoid horseshoe obstacles and other difficult situations for potential field planning. This includes planning a global path that will be large enough for the entire swarm to navigate without encountering difficult obstacles that are known failure points for the potential field method, like U-shaped horseshoe obstacles.

Another disadvantage of this biologically based approach is that it is local, reactive, and decentralized. This makes it difficult to incorporate higher-level considerations like optimizing routes for fuel efficiency. The tradeoff is greater robustness to limited communications, as will be shown later in the simulation results. To summarize, the primary advantage of the biologically inspired LF-APF is that the biological term creates a reactive, decentralized network of autonomous agents which is robust to loss of communication with the lead vehicle by any of the followers.

Another advantage of the LF-APF method is that by relying on a human-driven lead vehicle to set the desired path, many potential shortcomings of the APF method alone can be overcome. For example, the basic APF algorithm is known to struggle with horseshoe-shaped "C" obstacles. In the LF-APF method, it is assumed that the human driver functions as an effective global planner that avoids these terrain obstacles. The LF-APF method serves as a local planner that allows the following vehicles to effectively navigate the local terrain and interact with each other. The advantage of the biological term is that, should any one vehicle lose contact with the leader, it can still effectively move with the swarm using the reactive potential term from Eq. (5).

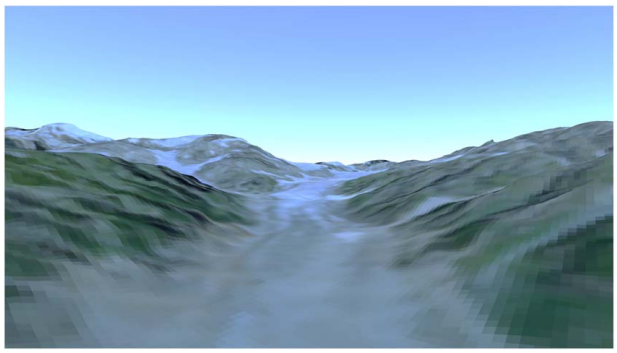

Fig. 3 The mountain pass terrain that the swarm was required to navigate

4 Experiments

The simulated experiments were implemented in ROS2 [62], which has some advantages over ROS for multi-robot operations. These include the ability to launch using PYTHON scripts, namespaces for groups of nodes, and the lack of requirement for a master node. The swarm consisted of teams of 2–9 MRZR-D4 vehicles equipped with an Ouster OS-2 64 beam lidar and a global position system (GPS)/inertial measurement unit (IMU) positioning system.

The autonomy stack consisted of three main modules—the global planning node, which used the blended LF-APF technique described in Sec. 3, the local planning node, which used a spline-based planner [63] to follow the global path based on the current state of the AGV. The pure-pursuit algorithm [64] was implemented as the vehicle controller. The controller output was steering on a range of $[-1, 1]$ of the maximum steering angle. Additionally, a PID controller was used for the throttle setting. Other than the new LF-APF node, the autonomy stack was similar to that described in our previous work [60,65].

4.1 Experiment Scenario. The terrain used for the experiment was a rocky mountain pass, as shown in Fig. 3. This terrain was chosen because of the large scale of the terrain and the significant elevation changes that pose particular communications challenges. In the experiment, the lead vehicle was driven by a human user through the pass while the rest of the vehicles followed the lead vehicle using the LF-APF algorithm described above. In order to facilitate repeated experimentation, the lead vehicle was driven only once, and then replays of that initial drive were used in subsequent simulations. The map size was 4 km^2, and the path length of the lead vehicle was 916 m.

There were 1–8 follow vehicles in the experiments (2–9 total vehicles) and they were equipped with simulated wireless radio transmitters. Each vehicle had an internal ROS2 namespace that included all of the autonomy messages related to local path planning and vehicle control. Each vehicle also had a communication node that received state updates from all the other robots, prefixed with their own namespaces. The state updates included the position and velocity in local East-North-Up coordinates.

The simulated 802.11 radios were given different maximum ranges in the simulation, ranging from 25 to 200 m. These ranges are typical for this type of wireless radio in outdoor use depending on the power, receiver sensitivity, and environmental conditions [66]. Five simulations were conducted for each radio distance and number of followers. This gave 200 total experiments. The experiments were randomized due to the random-test variable in the radio model as well as due to minor inconsistencies in the timing of message delivery in ROS2 between runs [62].

4.2 Metrics. Three performance metrics were considered for each simulation. The first was the mission success metric, which was the fraction of follower vehicles which successfully followed the leader through the mountain pass to the goal point. The second was formation keeping as measured by average vehicle spacing. The initial vehicle formation had a spacing of 6 m and the vehicles tended to space themselves out to the minimum spacing defined in Eq. (3) over the course of the experiment. However, if vehicles could not maintain formation, the average spacing would increase over the course of the simulation. Therefore, the ability to maintain the desired 16 meter spacing was the second metric.

The final metric was the total communication uptime. Because the communication links were one way, there were a total of $(n^2 - n)$ possible communication links for a swarm of n

total vehicles, including the follower. The number of connections was evaluated at each time-step, and the total was averaged for the duration of the simulation. The average number of connections divided by the maximum possible number of connections was taken to be the communication uptime.

4.3 Simulator. Realistic, physics-based simulation of AGV swarms presents a computational challenge due to the computing and memory requirements for simulating multiple vehicles—including the dynamics and sensors—using high-fidelity models. For this reason, many simulators used to study autonomous swarms have made simplifying assumptions, such as considering only two dimensions [67], to reduce the computational burden. In contrast, in this work we utilize high-HPC to enable physics-based simulation of up to nine vehicles at once in a ROS2 environment. The simulator used in this work is the MAVS [10]. MAVS is an open source simulation library for AGV that includes physics-based simulations of the terrain, tire, vehicle dynamics, environment conditions, and sensor performance like lidar and cameras. MAVS is cross-platform, optimized for use on high-performance computing, and ROS2 compatible, making it an ideal choice for the simulations in this work.

MAVS has been used to study several topics in AGV safety and performance including safety diagnostics [68], sensor placement [69], vehicle mobility through vegetation [70], AGV–pedestrian interaction [71], and simulating vehicle swarms [31]. MAVS realistic simulation of lidar accounts for beam divergence and target material properties including realistic interactions with vegetation [72] and rain [73]. These validation studies give confidence for the reliability of the results of this simulated study. The synthetic sensor data generation capability of MAVS has been used extensively in the training and testing of perception algorithms, including generating semantically labeled synthetic image data for training artificial intelligence algorithms [74,75] and generating labeled lidar point clouds for a similar purpose [76]. In addition, MAVS has recently been used as test environment for full stack autonomous navigation and validated against real-world experiments for estimating success rates at obstacle avoidance tasks [60,65]. Due to the extensive body of published research using MAVS, suitability for use with HPC and ROS2, and past success in using MAVS to study AGV swarms, MAVS was found to be the best choice for these experiments. In order to use ROS2 on HPC, we created a singularity container with ROS2, the MAVS simulator, and a ROS2 autonomy package using the LF-APF planner described above.

5 Results and Discussion

In this section, the simulation results are shown, and the relative advantages and opportunities for improvement are discussed.

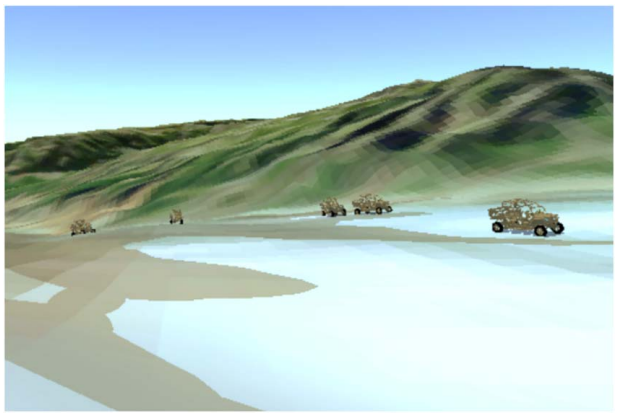

Fig. 4 Example simulation output with five vehicles; the leader vehicle is on the right of the image

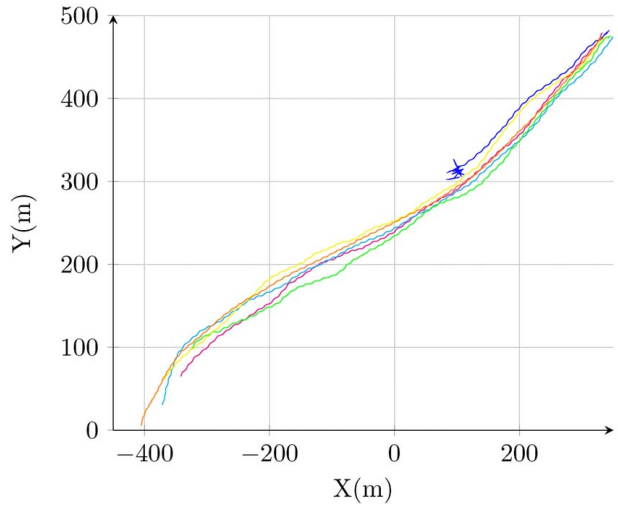

Fig. 5 Vehicle trajectories from a single experiment. Four of the five followers were successful, one was not.

5.1 Results. An example simulation with five vehicles is shown in Fig. 4. This figure demonstrates several qualitative observations that were made regarding the general characteristics of the LF-APF system. First, the lead vehicle had a tendency to pull away from the follower vehicles in the early part of the experiment, regardless of the number of vehicles. This was due to the relatively slowly changing leader potential function (Eq. (7)). The second general feature that is clear in Fig. 4 is the tendency of the follower vehicles to form pairs or clusters as the experiment progressed, as can be seen in the middle and left of the image. This is due to the inverse-range term in the attention factor in Eq. (6).

Each follower vehicle in the experiments could either succeed by reaching the endpoint of the mission or fail if it did not follow the leader to the endpoint. A set of trajectories from a single experiment with six vehicles and a communication range $r_n = 100$ m is shown in Fig. 5. In this figure, the vehicles travel southwest from upper right to lower left across the figure, with the goal point in the lower left corner. Figure 5 shows a case where four of the five following vehicles reached the goal and one (the blue trajectory) did not. This experiment therefore had a mission success rate of 0.8.

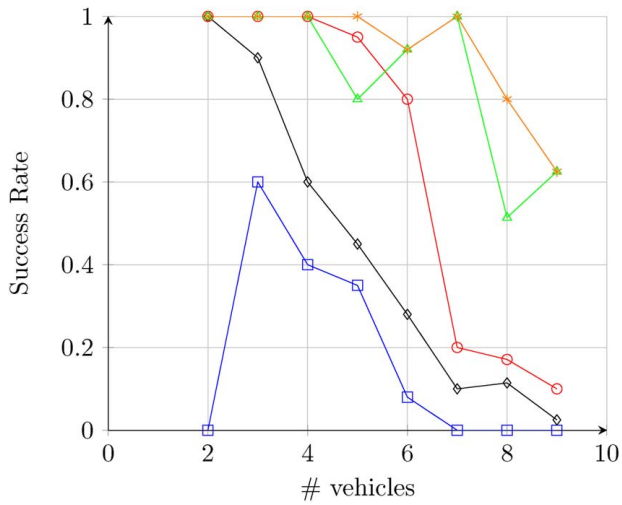

Fig. 6 Success rate versus number of vehicles for communication ranges of 25 m (blue squares), 50 m (black diamonds), 100 m (red circles), 200 m (green triangles), and 500 m (orange asterisks)

The average success rate for all swarm sizes and communication ranges is shown in Fig. 6. The rates were averaged across all five simulations for each combination of swarm size and radio range. Several conclusions can immediately be drawn from this figure. First, the success rate improves as the communication range increases—a result which is consistent with intuition.

Figure 6 shows that the highest success rate occurred when the radio range was 500 m. However, the success rate was still not 100% for 6, 7, and 9 vehicles even with this high communication range. This highlights another general observed feature of the LF-APF algorithm in this work. The attention weighted biological term (Eq. (6)) may cause following vehicles to abandon the leader in certain configurations that create a potential field that diverts them in another direction. If this diversion lasts long enough for the lead vehicle to leave the communication range of the follower vehicle, it may not recover. Even if it can recover, it may lose so much time that it does not reach the goal point by the end of the experiment, which occurred for the failures that accrued with 6, 7, and 9 vehicles at a radio range of 500 m. We observed that the larger the swarm became, the easier it was for the swarm to randomly divert a vehicle through collective motion that briefly outweighed the relatively strong potential force exerted by the leader. On the other hand, we observed that the collective motion of the following swarm also made it possible for a follower vehicle to reach its goal even when there was no direct connection with the lead vehicle simply by following the motion of the other nearby follower vehicles. This highlights the advantage of this decentralized approach.

Figure 7 shows the effectiveness of the swarm at maintaining a tight formation for different communication ranges and swarm sizes. Figure 7 shows that the two-vehicle system with a communication range of 25 m was the worst at holding formation. This makes sense because in this case there was only one follow vehicle and it was relatively easy for it to lose contact with the lead vehicle given the limited detection range. In this case, the follower vehicle became isolated and wandered aimlessly. This is also demonstrated by the 0% success rate in the 2-vehicle, 25 m radio range case. However, when the size of the system increases to at least three vehicles, the average spacing is reduced because the likelihood of maintaining communications with at least one partner is increased.

In contrast, all radio ranges showed the best formation keeping when there were three vehicles—one leader and two followers. This seems to be the ideal case for formation keeping because the follower vehicles can maintain communication with the leader easily (no need to spread out to accomodate a large number of vehicles) while also not being distracted by collective motions from a large group. Another feature that is apparent from Fig. 7 is that the formation control is optimal with $\geq$200 meter communication range, with little improvement for longer communication ranges. Finally, it is clear that the formation tends to spread out as the number of vehicles increases, as might be expected based on Eq. (3).

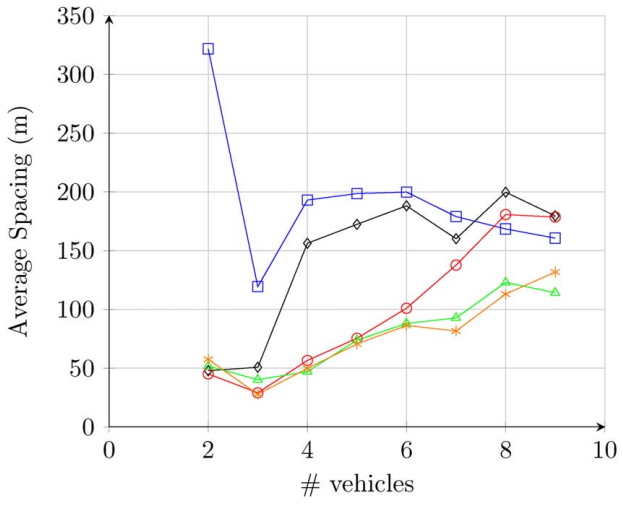

Fig. 7 Formation keeping versus number of vehicles for communication ranges of 25 m (blue squares), 50 m (black diamonds), 100 m (red circles), 200 m (green triangles), and 500 m (orange asterisks)

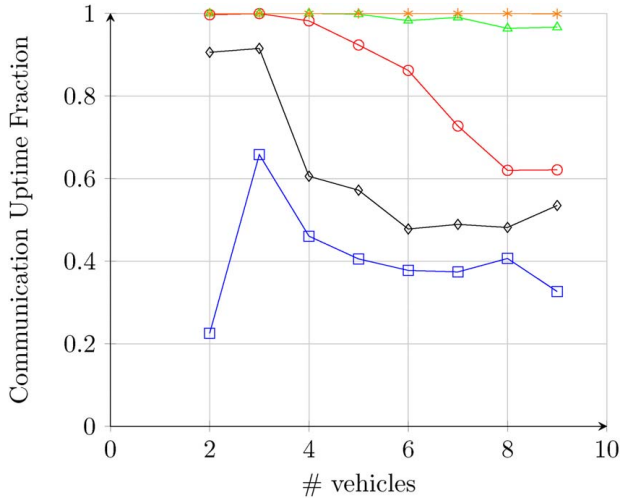

Fig. 8 Communication uptime fraction versus number of vehicles for communication ranges of 25 m (blue squares), 50 m (black diamonds), 100 m (red circles), 200 m (green triangles), and 500 m (orange asterisks)

Communication uptime as it depends on vehicle number is plotted for different radio ranges in Fig. 8. This figure shows the somewhat intuitive result that communication uptime increases as radio range increases, with little difference in uptime between the 200 m and 500 m radios, but significant differences between the 100 and 200 m radios. This suggests that the radio range needed for this blended, decentralized control algorithm is $\geq$200 m. Furthermore, it suggests that radio communication is not the only factor determining mission success for a vehicle, since some failures were observed for radio ranges of 200 m even though communication uptime was near 1 for all experiments at this radio range. As discussed above, these failures are due to the influence of the swarm over the other follower vehicles as the number of vehicles increases.

5.2 Discussion. From Fig. 6, it is clear that there are a limited number of circumstances where the success rate is 100%, meaning all the following vehicles reach the goal area. Clearly, communication range is a factor, with the success rate being quite low for all numbers of vehicles when the communication range is 25 m (blue squares). However, if the communication range is $\geq$100 m, the success rate is 100% for 2, 3, or 4 vehicles. This indicates that overall, the LF-APF method is effective for smaller numbers of vehicles if the communication range is adequate. However, Fig. 6 clearly shows a decrease in success rate as the number of vehicles increases. This is caused by the biological interaction term in Eq. (5). As is often seen in schools of fish or flocks of birds, as the size of the flock increases, it becomes likely that a small group may break away from the flock or school. This behavior was also observed in the simulations as the number of following vehicles increased. In fact, Ref. [9] found that the upper number limit for coordinated behavior in this type of biological interaction was 7, in agreement with our results. In contrast, other work using potential fields in swarm control used a predefined potential shape in order to control the distribution of the agents [14], in which case formation

control was maintained up to 10 robots. However, those methods do not have the reactive biological term of potential field used in this work.

While the failure rates at higher numbers of vehicles may indicate that the method presented in this work is inadequate for real applications, the strengths of the method (robust decentralized control that works in limited communication environments) indicate that there are some advantages and insights to be gained from the biologically informed blended leader–follower method, provided the failure rates can be reduced. Fortunately, there are several potential strategies for improving success rate result that may be explored in future work.

One strategy would be to include more than one human-driven vehicle in the swarm. Past research in this area has indicated that increasing the fraction of human-driven vehicles can improve the overall performance of the swarm [6]. Another potential mitigation strategy would be to provide the follower vehicles with some level of a priori mission awareness such as the GPS location of the final goal point that would allow clusters of vehicles that break away from the leader to continue to navigate toward the goal, and potentially rejoin the larger group.

Additionally, in future work we intend to investigate a modification of Eq. (7) where the entire motion history of the human-driven lead vehicle is included in the attractive potential. In this revised formulation, each point that the lead vehicle communicated to the swarm during its route would be maintained in the potential field as an attractive term. The magnitude of the attraction of each point would decrease over time, so that the most recent location would be the most attractive. We believe that this would allow vehicles that fall behind to eventually make their way back to the desired path and resume the desired trajectory toward the lead vehicle.

Also worth noting is the performance in ideal or infinite communication range. Figure 8 shows that for a communication range of 500 m (orange asterisks), the communication uptime was 100% for all cases, meaning that this was the best-case scenario with respect to communication. Even so, the success rate, which was 100% or near 100% for seven or fewer vehicles, decreased dramatically for eight and nine vehicles, indicating that as the size of the swarm increases, additional control strategies need to ensure 100% success, even if communication is ideal. However, it should be noted that even in relatively poor communication conditions, the success rate is fairly robust. For example, for the 25 m communication range (blue squares), for four vehicles, although the communication uptime was less than 50%, the success rate was still around 40%.

Another prominent feature of Figs. 6–8 is the discontinuity between two and three vehicles for the 25-m communication range scenario (blue squares). The blue squares in these figures show the results for different numbers of vehicles at a communication range of 25 m. At this relatively short communication range, it is easy for the follow vehicle to lose communications with the lead vehicle. With only two vehicles, once the communications link is broken, it cannot be reestablished easily in the absence of any other agents because the following vehicle has no goal point. However, once the total number of vehicles goes to three (one leader plus two autonomous followers) or more, if at least one of the followers still has contact with the leader, the biological, decentralized control algorithm will cause the other followers to "follow the follower." This results in the sharp discontinuity in the blue line. The effect is not nearly as pronounced when the communication range increases beyond 25 m. This highlights one of the advantages of the decentralized, biologically based algorithm proposed in this work—it allows swarms of vehicles to compensate for poor communication by reacting to the motion of their local neighbors.

Finally, from the data observed in Fig. 6, the following model for success rate (p_s) as a function of radio range (r_n) is proposed.

$$p_s(r_n, n_v) = 1 - e^{-\beta(n_v) r_n} \tag{12}$$

where the coefficient β is a function of the number of vehicles n_v

$$\beta(n_v) = \alpha\left(1 - \frac{1}{e^{-(n_v - n_0)}}\right) \tag{13}$$

and values of $\alpha = 0.033$ and $n_0 = 6.057$ were determined using least-squares fitting.

Equation (12) can be solved for r_n to determine the minimum required radio range ($r_{n,\text{req}}$ for a given number of vehicles and a desired success rate (or allowable failure rate)).

$$r_{\text{req}} = \ln\left(\frac{1}{\sqrt{[}\beta]1 - p_s}\right) \tag{14}$$

6 Summary and Conclusions

In summary, we developed a novel decentralized swarm control algorithm that used a blended LF-APF path planning approach, combined with attention-based swarm interactions to enable the navigation of a swarm of AGV through rough terrain using only a single lead vehicle and minimum point-to-point communication between vehicles. We systematically studied the influence of communication range on the performance of the system. Using repeated simulated experimentation, we evaluated the success of this approach for different numbers of vehicles (from 1 to 8 followers) and different radio communication ranges (25–200 m). We observed the general finding that small teams ($\leq$5 followers) work best since in larger teams it is easier for subgroups to break away from the leader. We also observed that increasing communication range is critical as the size of the swarm increases. A model for the minimum required radio range as a function of swarm size and desired success rate was developed from the measured data. This model can be used to inform future studies in the field of swarm robotics using decentralized communication and control strategies.

While this work revealed some positive aspects of the blended LF-APF method (decentralized control, robust to poor communications), it also showed that more work is necessary to improve the success rate as the number of vehicles increases. This includes improvements to the control process to increase the success rate, including introducing a persistent term to Eq. (7) that allows the entire trajectory history of the lead vehicle to be added to the attractive potential. Finally, time-variations on formation keeping will be studied to gain additional insight into the dynamic motion of the swarm. Additional future work in this area will include implementing the LF-APF algorithm on a swarm of remote control car sized (1/10 scale) AGV and performing testing in a variety of terrains and environments.

Acknowledgment

The research described and the resulting data presented herein, unless otherwise noted, were funded under PE 0602784A, Project T53 "Military Engineering Applied Research," Task 11.3 under Contract No. W56HZV-17-C-0095, managed by the U.S. Army Combat Capabilities Development Command (CCDC) and the Engineer Research and Development Center (ERDC). The work described in this document was conducted at the Center for Advanced Vehicular Systems, Mississippi State University. Permission was granted by ERDC to publish this information.

Conflict of Interest

There are no conflicts of interest.

Data Availability Statement

The datasets generated and supporting the findings of this article are obtainable from the corresponding author upon reasonable request.

References

[1] Daily, M., Medasani, S., Behringer, R., and Trivedi, M., 2017, "Self-driving Cars," Computer, **50**(12), pp. 18–23.

[2] Badue, C., Guidolini, R., Carneiro, R. V., Azevedo, P., Cardoso, V. B., Forechi, A., Jesus, L., Berriel, R., Paixão, T. M., and Mutz, F., 2020, "Self-driving Cars: A Survey," Exp. Syst. Appl., **165**(1), p. 113816.

[3] Kelly, A., Stentz, A., Amidi, O., Bode, M., Bradley, D., Diaz-Calderon, A., Happold, M., Herman, H., Mandelbaum, R., and Pilarski, T., 2006, "Toward Reliable Off Road Autonomous Vehicles Operating in Challenging Environments," Int. J. Rob. Res., **25**(5–6), pp. 449–483.

[4] Arnold, R., Carey, K., Abruzzo, B., and Korpela, C., 2019, "What Is a Robot Swarm: A Definition for Swarming Robotics," 2019 IEEE 10th Annual Ubiquitous Computing, Electronics & Mobile Communication Conference (UEMCON), New York, Oct. 10–12, IEEE, pp. 0074–0081.

[5] Sharkey, A. J., 2006, "Robots, Insects and Swarm Intelligence," Artif. Intell. Rev., **26**(1), pp. 255–268.

[6] Goodin, C., Prevost, Z., and Lemasson, B., 2015, "Simulation of Biologically-Inspired Control Algorithms for Teams of Ground Vehicles," Conference on Autonomous and Robotic Construction of Infrastructure, Ames, IA, p. 105.

[7] Kolling, A., Walker, P., Chakraborty, N., Sycara, K., and Lewis, M., 2015, "Human Interaction With Robot Swarms: A Survey," IEEE Trans. Human–Mach. Syst., **46**(1), pp. 9–26.

[8] Rohrig, C., and Telle, L., 2011, "Real-Time Communication and Localization for a Swarm of Mobile Robots Using IEEE 802.15. 4A CSS," 2011 IEEE Vehicular Technology Conference (VTC Fall), San Francisco, CA, Sept. 5–8, IEEE, pp. 1–5.

[9] Lemasson, B. H., Anderson, J. J., and Goodwin, R. A., 2013, "Motion-Guided Attention Promotes Adaptive Communications During Social Navigation," Proc. R. Soc. B: Biol. Sci., **280**(1754), p. 20122003.

[10] Hudson, C., Goodin, C., Miller, Z., Wheeler, W., and Carruth, D., 2020, "Mississippi State University Autonomous Vehicle Simulation Library," Proceedings of the Ground Vehicle Systems Engineering and Technology Symposium, Novi, MI, Aug. 10–12, pp. 11–13.

[11] Liu, Y., and Passino, K. M., 2000, "Swarm Intelligence: Literature Overview," Tech. Rep., The Ohio State University.

[12] Masar, M., 2013, "A Biologically Inspired Swarm Robot Coordination Algorithm for Exploration and Surveillance," 2013 IEEE 17th International Conference on Intelligent Engineering Systems (INES), San Jose, Costa Rica, June 19–21, IEEE, pp. 271–275.

[13] Parker, L. E., 2000, "Current State of the Art in Distributed Autonomous Mobile Robotics," Distributed Auton. Rob. Syst., **4**(1), pp. 3–12.

[14] Barnes, L., Fields, M., and Valavanis, K., 2007, "Unmanned Ground Vehicle Swarm Formation Control Using Potential Fields," 2007 Mediterranean Conference on Control & Automation, Athens, Greece, June 27–29, IEEE, pp. 1–8.

[15] Burgard, W., Moors, M., Fox, D., Simmons, R., and Thrun, S., 2000, "Collaborative Multi-robot Exploration," Proceedings 2000 ICRA. Millennium Conference. IEEE International Conference on Robotics and Automation. Symposia Proceedings (Cat. No. 00CH37065), San Francisco, CA, Apr. 24–28, Vol. 1, IEEE, pp. 476–481.

[16] Burgard, W., Moors, M., Stachniss, C., and Schneider, F. E., 2005, "Coordinated Multi-robot Exploration," IEEE Trans. Rob., **21**(3), pp. 376–386.

[17] Simmons, R., Apfelbaum, D., Burgard, W., Fox, D., Moors, M., Thrun, S., and Younes, H., 2000, "Coordination for Multi-robot Exploration and Mapping," AAAI/IAAI, Austin, TX, pp. 852–858.

[18] Thrun, S., Burgard, W., and Fox, D., 2000, "A Real-Time Algorithm for Mobile Robot Mapping With Applications to Multi-Robot and 3d Mapping," Proceedings 2000 ICRA. Millennium Conference. IEEE International Conference on Robotics and Automation. Symposia Proceedings (Cat. No. 00CH37065), San Francisco, CA, Apr. 24–28, Vol. 1, IEEE, pp. 321–328.

[19] Ko, J., Stewart, B., Fox, D., Konolige, K., and Limketkai, B., 2003, "A Practical, Decision-Theoretic Approach to Multi-robot Mapping and Exploration," Proceedings 2003 IEEE/RSJ International Conference on Intelligent Robots and Systems (IROS 2003), Las Vegas, NV, Vol. 4, IEEE, pp. 3232–3238.

[20] Howard, A., 2004, "Multi-robot Mapping Using Manifold Representations," IEEE International Conference on Robotics and Automation, 2004. Proceedings, New Orleans, LA, Vol. 4, IEEE, pp. 4198–4203.

[21] Eberhart, R., and Kennedy, J., 1995, "A New Optimizer Using Particle Swarm Theory," Proceedings of the Sixth International Symposium on Micro-machine and Human Science, MHS'95, Nagoya, Japan, Oct. 4–6, IEEE, pp. 39–43.

[22] Hereford, J. M., and Siebold, M. A., 2010, "Bio-inspired Search Strategies for Robot Swarms," Swarm Robotics, From Biology to Robotics, Alicante, Spain, pp. 1–27.

[23] Masár, M., and Zelenka, J., 2012, "Modification of PSO Algorithm for the Purpose of Space Exploration," 2012 IEEE 16th International Conference on Intelligent Engineering Systems (INES), Lisbon, Portugal, June 13–15, IEEE, pp. 51–54.

[24] Mabrouk, M., and McInnes, C., 2007, "Swarm Robot Social Potential Fields With Internal Agent Dynamics," 12th International Conference on Aerospace Sciences and Aviation Technology, ASAT-12, Cairo, Egypt.

[25] Dunbar, T. W., and Esposito, J. M., 2005, "Artificial Potential Field Controllers for Robust Communications in a Network of Swarm Robots," Proceedings of the Thirty-Seventh Southeastern Symposium on System Theory, 2005, SSST'05, Tuskeegee, AL, IEEE, pp. 401–405.

[26] Elkilany, B. G., Abouelsoud, A., and Fathelbab, A. M., 2017, "Adaptive Formation Control of Robot Swarms Using Optimized Potential Field Method," 2017 IEEE International Conference on Industrial Technology (ICIT), Toronto, Canada, Mar. 22–25, IEEE, pp. 721–725.

[27] Reynolds, C. W., 1987, "Flocks, Herds and Schools: A Distributed Behavioral Model," SIGGRAPH, New York.

[28] Dorigo, M., Birattari, M., and Stutzle, T., 2006, "Ant Colony Optimization," IEEE Comput. Intell. Mag., **1**(4), pp. 28–39.

[29] Ward, C. R., Gobet, F., and Kendall, G., 2001, "Evolving Collective Behavior in an Artificial Ecology," Artif. Life, **7**(2), pp. 191–209.

[30] Mississippi State University, 2018, https://www.hpc.msstate.edu/computing/.

[31] Goodin, C., Cagle, L., Henley, G., Fereday, R., Carrillo, J., Song, P., and McInnis, D., 2022, "Evaluating Tradeoffs for Swarm Reconnaissance With Autonomous Ground Vehicles," ASME J. Auton. Veh. Syst., **2**(1), p. 011002.

[32] Das, A. K., Fierro, R., Kumar, V., Ostrowski, J. P., Spletzer, J., and Taylor, C. J., 2002, "A Vision-Based Formation Control Framework," IEEE Trans. Rob. Autom., **18**(5), pp. 813–825.

[33] Penghao, W., and Zhiyong, G., 2016, "Leader–Follower Formation Control of Multi-robot Systems Using the Dynamic Surface Approach," 2016 35th Chinese Control Conference (CCC), Nadi, Fiji, IEEE, pp. 7757–7762.

[34] Dehghani, M. A., Menhaj, M. B., and Azimi, M., 2016, "Leader–Follower Formation Control Using an Onboard Leader Tracker," 2016 4th International Conference on Control, Instrumentation, and Automation (ICCIA), Guilin, China, IEEE, pp. 99–104.

[35] Miah, M. S., 2018, "Leader–Follower Localization and Mapping Using Range-Only Measurements," IECON 2018-44th Annual Conference of the IEEE Industrial Electronics Society, Washington, DC, IEEE, pp. 2570–2575.

[36] Tutuko, B., Nurmaini, S., and Fitriana, G. F., 2017, "Tracking Control Enhancement on Non-holonomic Leader–Follower Robot," 2017 International Conference on Electrical Engineering and Computer Science (ICECOS), Palembang, Indonesia, Aug. 22–23, pp. 83–86.

[37] Mendel, J. M., 2013, "General Type-2 Fuzzy Logic Systems Made Simple: A Tutorial," IEEE Trans. Fuzzy Syst., **22**(5), pp. 1162–1182.

[38] Quigley, M., Conley, K., Gerkey, B., Faust, J., Foote, T., Leibs, J., Wheeler, R., and Ng, A. Y., 2009, "Ros: An Open-Source Robot Operating System," ICRA Workshop on Open Source Software, Kobe, Japan, May 12, p. 5.

[39] de Souza Neto, A. M., and Romero, R. A. F., 2019, "A Decentralized Approach to Drone Formation Based on Leader–Follower Technique," 2019 Latin American Robotics Symposium (LARS), 2019 Brazilian Symposium on Robotics (SBR) and 2019 Workshop on Robotics in Education (WRE), Rio Grande, Brazil, IEEE, pp. 358–362.

[40] Zhang, X., Ma, H., and Wang, J., 2017, "Decentralized Adaptive Control of a Class of Discrete-Time Nonlinear Hidden-Leader Follower Multi-agent Systems," 36th Chinese Control Conference (CCC), Chongqing, China, June 26–28, IEEE, pp. 3593–3598.

[41] Xia, Y., Zheng, Y., Wang, X., Zhang, L., and Wang, L., 2021, "Research on Path Planning Algorithm of Service Robot in Dynamic Environment," 2021 3rd International Conference on Artificial Intelligence and Advanced Manufacture (AIAM), Manchester, UK, IEEE, pp. 478–485.

[42] Siegwart, R., Nourbakhsh, I. R., and Scaramuzza, D., 2011, *Introduction to Autonomous Mobile Robots*, MIT Press, Cambridge, MA.

[43] Zamirian, M., Kamyad, A., and Farahi, M., 2009, "A Novel Algorithm for Solving Optimal Path Planning Problems Based on Parametrization Method and Fuzzy Aggregation," Phys. Lett. A, **373**(38), pp. 3439–3449.

[44] Mineo, C., Pierce, S. G., Wright, B., Nicholson, P. I., and Cooper, I., 2015, "Robotic Path Planning for Non-destructive Testing of Complex Shaped Surfaces," AIP Conference Proceedings, Minneapolis, MN, pp. 1977–1987.

[45] Jia, Y.-h., and Mei, F.-x., 2002, "Simple Path Planning for Mobile Robots in the Present of Obstacles," J.-Beijing Inst. Technol. English Edition, **11**(2; ISSU 32), pp. 208–211.

[46] Orozco-Rosas, U., Montiel, O., and Sepúlveda, R., 2019, "Mobile Robot Path Planning Using Membrane Evolutionary Artificial Potential Field," Appl. Soft Comput., **77**(1), pp. 236–251.

[47] Khatib, O., 1986, "Real-Time Obstacle Avoidance for Manipulators and Mobile Robots," Int. J. Rob. Res., **5**(1), pp. 90–98.

[48] Zhang, Z., Chen, S., Li, Y., Wang, L., Ren, R., Xu, L., Wang, J., and Zhang, X., 2022, "Local Path Planning of Unmanned Underwater Vehicle Based on Improved APF and Rolling Window Method," 2022 International Conference on Cyber-physical Social Intelligence (ICCSI), Nanjing, China, Nov. 18–21, IEEE, pp. 542–549.

[49] Imran, M., and Kunwar, F., 2016, "A Hybrid Path Planning Technique Developed by Integrating Global and Local Path Planner," 2016 International Conference on Intelligent Systems Engineering (ICISE), Los Angeles, CA, Apr. 20–22, IEEE, pp. 118–122.

[50] Ji, Y., Ni, L., Zhao, C., Lei, C., Du, Y., and Wang, W., 2023, "Tripfield: A 3d Potential Field Model and Its Applications to Local Path Planning of Autonomous Vehicles," IEEE Trans. Intell. Transp. Syst., **24**(3), pp. 3541–3554.

[51] Ragavan, S. V., Ponnambalam, S., and Sumero, C., 2011, "Waypoint-Based Path Planner for Mobile Robot Navigation Using PSO and Ga-ais," 2011 IEEE Recent Advances in Intelligent Computational Systems, Trivandrum, India, Sept. 22–24, IEEE, pp. 756–760.
[52] Warren, C. W., 1989, "Global Path Planning Using Artificial Potential Fields," 1989 IEEE International Conference on Robotics and Automation, Scottsdale, AZ, May 14–19, pp. 7316–7317.
[53] Barraquand, J., Langlois, B., and Latombe, J.-C., 1992, "Numerical Potential Field Techniques for Robot Path Planning," IEEE Trans. Syst. Man Cybern., **22**(2), pp. 224–241.
[54] Hwang, Y. K., and Ahuja, N., 1992, "A Potential Field Approach to Path Planning," IEEE Trans. Rob. Autom., **8**(1), pp. 23–32.
[55] Raja, P., and Pugazhenthi, S., 2012, "Optimal Path Planning of Mobile Robots: A Review," Int. J. Phys. Sci., **7**(9), pp. 1314–1320.
[56] Elfes, A., 1989, "Using Occupancy Grids for Mobile Robot Perception and Navigation," Computer, **22**(6), pp. 46–57.
[57] Collins, T., and Collins, J., 2007, "Occupancy Grid Mapping: An Empirical Evaluation," 2007 Mediterranean Conference on Control & Automation, Athens, Greece, IEEE, pp. 1–6.
[58] Konolige, K., Agrawal, M., Blas, M. R., Bolles, R. C., Gerkey, B., Sola, J., and Sundaresan, A., 2009, "Mapping, Navigation, and Learning for Off-Road Traversal," J. Field Rob., **26**(1), pp. 88–113.
[59] Goodin, C., Dabbiru, L., Hudson, C., Mason, G., Carruth, D., and Doude, M., 2021, "Fast Terrain Traversability Estimation With Terrestrial Lidar in Off-Road Autonomous Navigation," SPIE DCS, Orlando, FL, pp. 189–199.
[60] Carruth, D., Goodin, C., Dabbiru, L., Scherer, N., and Jayakumar, P., 2020, "Predicting Error Propagation in Autonomous Ground Vehicle Subsystems," Proceedings of the Ground Vehicle Systems Engineering and Technology Symposium, Novi, MI, pp. 11–13.
[61] Aust, S., Prasad, R. V., and Niemegeers, I. G., 2015, "Outdoor Long-Range Wlans: A Lesson for IEEE 802.11 Ah," IEEE Commun. Surv. Tutorials, **17**(3), pp. 1761–1775.
[62] Maruyama, Y., Kato, S., and Azumi, T., 2016, "Exploring the Performance of ROS2," Proceedings of the 13th International Conference on Embedded Software, Pittsburgh, PA, pp. 1–10.
[63] Hu, X., Chen, L., Tang, B., Cao, D., and He, H., 2018, "Dynamic Path Planning for Autonomous Driving on Various Roads With Avoidance of Static and Moving Obstacles," Mech. Syst. Signal Process., **100**(1), pp. 482–500.
[64] Coulter, R. C., 1992, "Implementation of the Pure Pursuit Path Tracking Algorithm," Tech. Rep., Carnegie-Mellon UNIV Pittsburgh PA Robotics INST.
[65] Goodin, C., Carruth, D. W., Dabbiru, L., Hudson, C. H., Cagle, L. D., Scherrer, N., Moore, M. N., and Jayakumar, P., 2022, "Simulation-Based Testing of Autonomous Ground Vehicles," Autonomous Systems: Sensors, Processing and Security for Ground, Air, Sea and Space Vehicles and Infrastructure 2022, Orlando, FL, Vol. 12115, SPIE, pp. 167–174.
[66] Zhou, T., Sharif, H., Hempel, M., Mahasukhon, P., Wang, W., and Ma, T., 2009, "A Deterministic Approach to Evaluate Path Loss Exponents in Large-Scale Outdoor 802.11 Wlans," 2009 IEEE 34th Conference on Local Computer Networks, Zurich, Switzerland, Oct. 20–23, IEEE, pp. 348–351.
[67] Atyabi, A., Anderson, T. A., Treharne, K., and Powers, D. M., 2010, "Magician Simulator," ICARV, Singapore.
[68] Dantuluri, N. A. V., and Pisu, P., 2021, "Safety Diagnostics and Degraded Operational Modes for Off-Road Unmanned Ground Combat Vehicles," Annual Conference of the PHM Society, Nashville, TN.
[69] Meadows, W., Hudson, C., Goodin, C., Dabbiru, L., Powell, B., Doude, M., Carruth, D., Islam, M., Ball, J. E., and Tang, B., 2019, "Multi-Lidar Placement, Calibration, Co-Registration, and Processing on a Subaru Forester for Off-Road Autonomous Vehicles Operations," Autonomous Systems: Sensors, Processing, and Security for Vehicles and Infrastructure 2019, Orlando, FL.
[70] Hudson, C. R., 2022, *The Effects of Ecological Simulation for Ground Vehicle Mobility Forecasting*, Mississippi State University, Starkville, MS.
[71] Hudson, C. R., Deb, S., Goodin, C., and Carruth, D. W., 2020, "Using VR Generated Pedestrian Behaviors in Autonomous Vehicle Simulations," Advances in Human Factors and Systems Interaction: Proceedings of the AHFE 2020 Virtual Conference on Human Factors and Systems Interaction, San Diego, CA, July 16–20, Springer, pp. 303–308.
[72] Goodin, C., Doude, M., Hudson, C., and Carruth, D., 2018, "Enabling Off-Road Autonomous Navigation-Simulation of Lidar in Dense Vegetation," Electronics, **7**(9), p. 154.
[73] Goodin, C., Carruth, D., Doude, M., and Hudson, C., 2019, "Predicting the Influence of Rain on Lidar in Adas," Electronics, **8**(1), p. 89.
[74] Goodin, C., Sharma, S., Doude, M., Carruth, D., Dabbiru, L., and Hudson, C., 2019, "Training of Neural Networks With Automated Labeling of Simulated Sensor Data," Tech. Rep., SAE Technical Paper.
[75] Boone, J., Goodin, C., Dabbiru, L., Hudson, C., Cagle, L., and Carruth, D., 2022, "Training Artificial Intelligence Algorithms With Automatically Labelled UAV Data From Physics-Based Simulation Software," Appl. Sci., **13**(1), p. 131.
[76] Dabbiru, L., Goodin, C., Scherrer, N., and Carruth, D., 2020, "Lidar Data Segmentation in Off-Road Environment Using Convolutional Neural Networks (CNN)," SAE Int. J. Adv. Curr. Pract. Mob., **2**(6), pp. 3288–3292.